responsible for the difference in bond angles between it and the other more related derivatives.

Acknowledgment. The support of this research by the National Science Foundation (Grant CHE8504737) is gratefully acknowledged. We also thank the University of Massachusetts Computing Center for generous allocation of computer time.

Supplementary Material Available: Thermal parameters and additional bond lengths and angles (Tables S1 and S2, respectively, for **1**, Tables S3 and S5 for **2**, Tables S6 and S7 for **3**) and fixed hydrogen atom parameters for **2** (Table S4) (8 pages); listings of calculated and observed structure factor amplitudes for **1-3** (32 pages). Ordering information is given on any current masthead page.

Photoinduced Intramolecular Electron Transfer in Peptide-Bridged Molecules

Kirk S. Schanze*[1] and Kenneth Sauer

Contribution from the Department of Chemistry and Laboratory of Chemical Biodynamics, Lawrence Berkeley Laboratory, University of California, Berkeley, California 94720.
Received August 11, 1986

Abstract: Two series of molecules have been prepared and characterized in which a polypyridyl Ru(II) complex is linked to *p*-dimethoxybenzene (DMB) and *p*-benzoquinone (Q) moieties by peptide bridges containing the amino acid L-proline (Pro). The photophysical properties of the metal-to-ligand charge transfer (MLCT) excited state of the Ru(II) chromophore have been examined for the complexes with 0, 1, 2, 3, and 4 intervening Pro residues. Steady state and time resolved luminescence experiments on the Pro-bridged DMB system show that the properties of the Ru MLCT excited state are only slightly modified from those of an unsubstituted model complex by the presence of covalently attached DMB peptides. Experiments on the Pro-bridged Ru-Q complexes show that the Q site quenches the yield and lifetime of the Ru MLCT emission. Furthermore, the quenching efficiency is diminished as the number of peptide spacers is increased. The quenching process is ascribed to long-range intramolecular Ru-to-Q electron transfer. This hypothesis is supported by time-resolved luminescence data which suggest that the average electron transfer rate falls sharply with an increase in the peptide bridge length.

There has been considerable interest recently in exploring the role of distance in the rate of electron transfer between donor and acceptor sites that are spatially separated.[2] Studies involving various chemical and physical approaches have addressed this important problem. Rates have been measured for electron transfer between donor and acceptor sites that are randomly distributed in glassy matrices,[3-5] held at fixed distances by protein frameworks[4c,6-8] or between sites that are separated by peptide oligomers,[10] rigid carbon-carbon bond frameworks,[11-16] or by various aliphatic[17,18] and aromatic spacers.[19] Several goals are

Scheme I

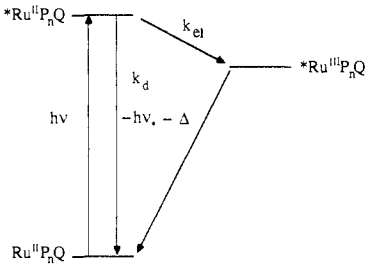

(1) Present address: Department of Chemistry, University of Florida, Gainesville, FL 32611.

(2) For reviews, see: (a) Marcus, R. A.; Sutin, N. *Biochim. Biophys. Acta* **1985**, *811*, 265-322. (b) Newton, M. D.; Sutin, N. *Annu. Rev. Phys. Chem.* **1984**, *35*, 437-480. (c) De Vault, D. *Quantum-Mechanical Tunnelling in Biological Systems*; 2nd ed.; Cambridge University Press: New York, 1984.

(3) (a) Beitz, J. V.; Miller, J. R. *J. Chem. Phys.* **1979**, *71*, 4579-4595. (b) Miller, J. R.; Beitz, J. V. *J. Chem. Phys.* **1981**, *74*, 6746-6756. (c) Miller, J. R.; Beitz, J. V.; Huddleston, R. K. *J. Am. Chem. Soc.* **1984**, *106*, 5057-5068. (d) Miller, J. R.; Hartman, K. R.; Abrash, S. *J. Am. Chem. Soc.* **1982**, *104*, 4296-4298.

(4) (a) Strauch, S.; McLendon, G.; McGuire, M.; Guarr, T. *J. Phys. Chem.* **1983**, *87*, 3579-3581. (b) Guarr, T.; McGuire, M.; McLendon, G. *J. Am. Chem. Soc.* **1985**, *107*, 5104-5111. (c) McLendon, G.; Guarr, T.; McGuire, M.; Simolo, K.; Strauch, S.; Taylor, K. *Coord. Chem. Rev.* **1985**, *64*, 113-124.

(5) Domingue, R. P.; Fayer, M. D. *J. Chem. Phys.* **1985**, *83*, 2242-2251.

(6) (a) Winkler, J. R.; Nocera, D. G.; Yocum, K. M.; Bordignon, E.; Gray, H. B. *J. Am. Chem. Soc.* **1982**, *104*, 5798-5800. (b) Nocera, D. G.; Winkler, J. R.; Yocum, K. M.; Bordignon, E.; Gray, H. B. *J. Am. Chem. Soc.* **1984**, *106*, 5145-5150. (c) Crutchley, R. J.; Ellis, W. R., Jr.; Gray, H. B. *J. Am. Chem. Soc.* **1985**, *107*, 5002-5004. (d) Kostic, N. M.; Margalit, R.; Che, C.-M.; Gray, H. B. *J. Am. Chem. Soc.* **1983**, *105*, 7765-7767. (e) Mayo, S. L.; Ellis, W. R., Jr.; Crutchley, R. J.; Gray, H. B. *Science* **1986**, *233*, 948-952.

(7) (a) McGourty, J. L.; Blough, N. V.; Hoffman, B. M. *J. Am. Chem. Soc.* **1983**, *105*, 4470-4472. (b) Peterson-Kennedy, S. E.; McGourty, J. L.; Hoffman, B. M. *J. Am. Chem. Soc.* **1984**, *106*, 5010-5012. (c) Peterson-Kennedy, S. E.; McGourty, J. L.; Ho, P. S.; Sutoris, C. J.; Liang, N.; Zemel, H.; Blough, N. V.; Margoliash, E.; Hoffman, B. M. *Coord. Chem. Rev.* **1985**, *64*, 125-133.

(8) (a) McLendon, G. L.; Winkler, J. R.; Nocera, D. G.; Mauk, M. R.; Mauk, A. G.; Gray, H. B. *J. Am. Chem. Soc.* **1985**, *107*, 739-740. (b) McLendon, G.; Miller, J. R. *J. Am. Chem. Soc.* **1985**, *107*, 7811-7816. (c) Simolo, K. P.; McLendon, G. L.; Mauk, M. R.; Mauk, A. G. *J. Am. Chem. Soc.* **1984**, *106*, 5012-5013.

(9) (a) Isied, S. S.; Kuehn, C.; Worosila, G. *J. Am. Chem. Soc.* **1984**, *106*, 1722-1726.

(10) (a) Isied, S. S.; Vassilian, A. *J. Am. Chem. Soc.* **1984**, *106*, 1726-1732. (b) Isied, S. S.; Vassilian, A. *J. Am. Chem. Soc.* **1984**, *106*, 1732-1736. (c) Isied, S. S.; Vassilian, A.; Magnuson, R. H.; Schwartz, H. A. *J. Am. Chem. Soc.* **1985**, *107*, 7432-7438.

(11) (a) Calcaterra, L. T.; Closs, G. L.; Miller, J. R. *J. Am. Chem. Soc.* **1983**, *105*, 670-671. (b) Miller, J. R.; Calcaterra, L. T.; Closs, G. L. *J. Am. Chem. Soc.* **1984**, *106*, 3047-3049. (c) Closs, G. L.; Calcaterra, L. T.; Green, N. J.; Penfield, K. W.; Miller, J. R. *J. Phys. Chem.* **1986**, *90*, 3673-3683. (d) Penfield, K. W.; Miller, J. R.; Paddon-Row, M. N.; Cotsaris, E.; Oliver, A. M; Hush, N. S. *J. Am. Chem. Soc.* **1987**, *109*, 5061-5065.

(12) (a) Pasman, P.; Koper, N. W.; Verhoeven, J. W. *Recl. Trav. Chim. Pays-Bas* **1982**, *101*, 363-364. (b) Pasman, P.; Mes, G. F.; Koper, N. W.; Verhoeven, J. W. *J. Am. Chem. Soc.* **1985**, *107*, 5839-5843.

(13) (a) Wasielewski, M. R.; Niemczyk, M. P. *J. Am. Chem. Soc.* **1984**, *106*, 5043-5045. (b) Wasielewski, M. R.; Niemczyk, M. P.; Svec, W. A.; Pewitt, E. B. *J. Am. Chem. Soc.* **1985**, *107*, 1080-1082. (c) Wasielewski, M. R.; Niemczyk, M. P.; Svec, W. A.; Pewitt, E. B. *J. Am. Chem. Soc.* **1985**, *107*, 5562-5563.

(14) (a) Hush, N. S. *Coord. Chem. Rev.* **1985**, *64*, 135-157. (b) Oevering, H.; Paddon-Row, M. N.; Heppener, M.; Oliver, A. M.; Cotsaris, E.; Verhoeven, J. W.; Hush, N. S. *J. Am. Chem. Soc.* **1987**, *109*, 3258-3269.

(15) (a) Joran, A. D.; Leland, B. A.; Geller, G. G.; Hopfield, J. J.; Dervan, P. B. *J. Am. Chem. Soc.* **1984**, *106*, 6090-6092. (b) Leland, B. A.; Joran, A. D.; Felker, P. M.; Hopfield, J. J.; Zewail, A. H.; Dervan, P. B. *J. Phys. Chem.* **1985**, *89*, 5571-5573.

0002-7863/88/1510-1180$01.50/0

common to each of these studies: to establish quantitatively the dependence of the electron transfer rate on the distance between donor and acceptor sites,[2a] to determine the relation between distance dependence and reaction driving force,[2a,3b,4b,20] and to learn how the composition of the molecular framework, spacer, or solvent, which separates the donor and acceptor, affects the distance dependence.[14a]

Pioneering work on intramolecular energy transfer suggested that oligopeptides which contain repeating L-proline units could be useful as spacers by allowing systematic variation in the distance between terminal pendant groups.[21] Taking this lead, Isied and co-workers recently demonstrated that oligo(L-proline) can be useful as a spacer in the study of intramolecular electron transfer reactions.[10b,c] Although the donor–acceptor systems designed by Isied's group demonstrate the utility of peptide spacers, their results are difficult to interpret because in several instances intramolecular electron transfer rates are slow, allowing competition from peptide conformational isomerization and bimolecular electron transfer paths. Clearly, it would be desirable to develop a system that utilizes an oligopeptide spacer but which has an intrinsically higher rate for electron transfer.[10b,c]

We have designed and characterized a system that utilizes a series of oligo(L-proline) spacers to separate an electron donor and acceptor pair which under favorable conditions undergo an exceedingly rapid electron transfer reaction. The system is based on the use of an electronically excited state as electron donor. Recent experiments have proven that such systems can be extremely useful in the study of fast electron transfer reactions because the reactant, *D–A, is photochemically excited and the kinetics of its decay by intramolecular electron transfer to the product, D^+–A^-, are readily monitored by time resolved emission or absorption techniques.[12-19] The system described herein utilizes a polypyridyl Ru(II) complex as a photoexcited electron donor and a *p*-benzoquinone moiety as an electron acceptor. The rate of photoinduced intramolecular Ru to quinone electron transfer (k_{et} process, Scheme I) can be deduced from emission experiments. The Ru(II) complex was selected because its lowest excited state is based on a metal-to-ligand charge transfer (MLCT) transition and therefore displays features amenable to the study of intramolecular electron transfer reactions: (1) MLCT excited states are strongly redox active—indeed, $*Ru(bpy)_3^{2+}$ is both a good oxidant and a good reductant.[22] (2) Polypyridine Ru(II) MLCT excited states are luminescent, allowing measurement of excited state kinetics with time resolved luminescence techniques.[23] (3) MLCT excited states are relatively long lived, allowing reactions with comparatively slow kinetics to compete effectively with normal excited state decay processes.[23] The quinone moiety was chosen as acceptor due to its facile reduction[24] and because of its importance as an electron acceptor in many biological redox systems.[25]

Chart I

Structures and Abbreviations

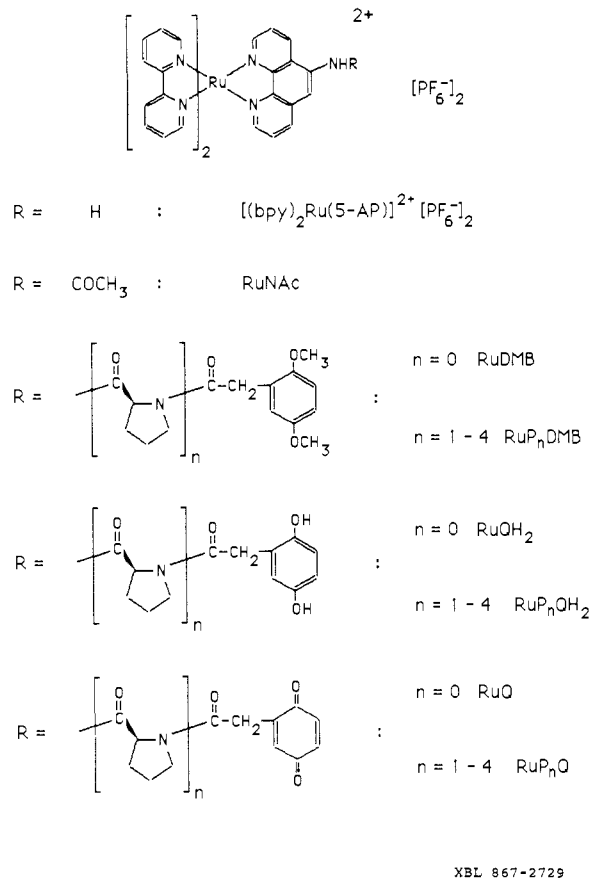

This report describes the characterization and photophysical properties of two series of peptide-bridged complexes, RuP_nDMB and RuP_nQ (see structures and abbreviations for definition of the nomenclature used throughout, Chart I).[26] The RuP_nDMB system was examined to provide information regarding the effect of the peptide upon the normal decay parameters of the Ru MLCT excited state. Results on the RuP_nQ system show that the rate of Ru to quinone electron transfer is strongly affected by the number of intervening peptide spacers.

Results and Discussion

Synthesis and Characterization of the Peptide-Linked Complexes. The general strategy for synthesis of the Ru–quinone complexes followed techniques developed for synthesis of amide and ester linked porphyrin–quinone molecules.[27,28] A detailed description of the synthetic methods and analytical results is given in the Experimental Section; aspects of the sythesis which are relevant to the photophysical experiments follow. The preparative scheme involved the sequence $RuP_nDMB \rightarrow RuP_nQH_2 \rightarrow RuP_nQ$. The RuP_nQH_2 complexes were carefully purified by repeated chromatography and fully characterized by ^{13}C and ^1H NMR, FTIR, UV–vis, and elemental analysis. Following oxidation, the RuP_nQ complexes were characterized by ^1H NMR and UV–vis spectroscopy. These techniques established that (1) oxidation could be effected in 90–95% yield and (2) the quinone complexes were free of all impurities except slight contamination by residual RuP_nQH_2. Attempts to purify the RuP_nQ complexes by a variety of techniques invariably resulted in complete reduction of the

(16) Bolton, J. R.; Ho, T.-F.; Liauw, S.; Siemiarczuk, A.; Wan, C. S. K.; Weedon, A. C. *J. Chem. Soc. Chem. Commun.* **1985**, 559–560.
(17) (a) McIntosh, A. R.; Siemiarczuk, A.; Bolton, J. R.; Stillman, M. J.; Ho, T.-F.; Weedon, A. C. *J. Am. Chem. Soc.* **1983**, *105*, 7215–7223. (b) Siemiarczuk, A.; McIntosh, A. R.; Ho T.-F.; Stillman, M. J.; Roach, K. J.; Weedon, A. C.; Bolton, J. R.; Connolly, J. C. *J. Am. Chem. Soc.* **1983**, *105*, 7224–7230. (c) Schmidt, J. A.; Siemiarczuk, A.; Weedon, A. C.; Bolton, J. R. *J. Am. Chem. Soc.* **1985**, *107*, 6112–6114.
(18) Moore, T. A.; Gust, D.; Mathis, P.; Mialocq, J.-C.; Chachaty, C.; Bensasson, R. V.; Land, E. J.; Doizi, D.; Liddell, P. A.; Lehman, W. R.; Nemeth, G. A.; Moore, A. L. *Nature (London)* **1984**, *307*, 630–632.
(19) Heitele, H.; Michel-Beyerle, M. E. *J. Am. Chem. Soc.* **1985**, *107*, 8286–8288.
(20) Brunschwig, B. S.; Ehrenson, S.; Sutin, N. *J. Am. Chem. Soc.* **1984**, *106*, 6858–6859.
(21) (a) Stryer, L.; Haugland, R. P. *Proc. Natl. Acad. Sci. U.S.A.* **1967**, *58*, 719–726. (b) Gabor, G. *Biopolymers* **1968**, *6*, 809–816.
(22) Bock, C. R.; Connor, J. A.; Gutierrez, A. R.; Meyer, T. J.; Whitten, D. G.; Sullivan, B. P.; Nagle, J. K. *J. Am. Chem. Soc.* **1979**, *101*, 4815–4824.
(23) Caspar, J. V.; Meyer, T. J. *J. Am. Chem. Soc.* **1983**, *105*, 5583–5590.
(24) Wilford, J. H.; Archer, M. D.; Bolton, J. R.; Ho, T.-F.; Schmidt, J. A.; Weedon, A. C. *J. Phys. Chem.* **1985**, *89*, 5395–5398.
(25) Trumpower, B. L. *Function of Quinones in Energy Conserving Systems*; Academic: New York, 1982.

(26) Abbreviations used throughout this paper: bpy = 2,2'-bipyridine; 5-AP = 5-amino-1,10-phenanthroline; DMB = (2,5-dimethoxyphenyl)acetyl; QH_2 = (2,5-dihydroxyphenyl)acetyl; Q = (2,5-benzoquinyl)acetyl; OBz = benzyloxy.
(27) Kong, J. L. Y.; Loach, P. A. *J. Heterocycl. Chem.* **1980**, *17*, 737–744.
(28) Ho, T.-F.; McIntosh, A. R.; Weedon, A. C. *Can. J. Chem.* **1984**, *62*, 967–974.

Table I. Steady State Emission Maxima and Intensities, CH_2Cl_2 Solution[a,b]

	complex		
n	RuNAc	RuP_nDMB	RuP_nQ
0	1.00 (599)	1.11 (599)	0.045 (598)
1		—	0.056 (601)
2		1.10 (602)	0.10 (602)
3		1.19 (603)	0.33 (602)
4		1.01 (601)	0.53 (600)

[a] Intensities for emission at 600 nm relative to RuNAc. Estimated error ±10%. Emission wavelength maxima in nm given in parentheses. [b] λ_{ex} = 450 nm. λ_{em} = 600 nm.

quinone. As a result, the luminescence experiments were carried out on RuP_nQ samples that contained 5–10% residual RuP_nQH_2. The effects of this impurity on the photophysics are discussed below.

Electrochemistry. Energetics of Excited State Electron Transfer. The excited state redox potentials for the Ru chromophore common to each of the complexes can be calculated from electrochemical data and the MLCT excited state energy. Cyclic voltammetry of RuNAc, RuDMB, and RuQ reveals that the first oxidation and reduction potentials for the Ru center common to each of the complexes are +1.25 and −1.35 V, respectively (potentials vs SSCE). From these redox potentials and the MLCT excited state energy (2.1 eV) the following excited state potentials are calculated: $E_{1/2}(*Ru^{2+}/Ru^{3+}) = -0.85$ V; $E_{1/2}(*Ru^{2+}/Ru^{+}) = +0.75$ V.[29] These potentials indicate that an electron acceptor with a reduction potential >−0.85 V or an electron donor with an oxidation potential <+0.75 V will quench the MLCT excited state by electron transfer.

Cyclic voltammetry on RuDMB reveals that the DMB functional group is not redox active within the potential window −1.5 to +1.7 V. This indicates that the DMB functional group cannot quench the Ru MLCT excited state by thermodynamically favorable electron transfer.

Cyclic voltammetry of RuQ reveals that in addition to the characteristic waves for the Ru complex an irreversible cathodic wave is observed at $E_p = -0.45$ V. This wave is associated with reduction of the quinone functional group. The irreversibility indicates that chemical reactions of the quinone radical anion are significant on the time scale of the electrochemical experiment. Under these conditions the peak potential for the observed wave only approximates the true thermodynamic potential for the electrode process.[30] However, measurements on very similar quinones suggest that $E_{1/2}(Q/Q^{\bullet-}) \approx -0.50$ V.[24] From this potential along with the excited state oxidation potential for the Ru complex, $E_{1/2}(*Ru^{2+}/Ru^{3+}) = -0.85$ V, the free energy for *Ru to quinone electron transfer (k_{et} process, Scheme I) is estimated to be −0.35 eV.

Luminescence Spectra and Quantum Yields. Steady state emission spectra were obtained for each of the Ru complexes in vacuum degassed CH_2Cl_2. Table I contains a summary of emission maxima and relative quantum yields.

The emission energy and bandshapes for RuNAc and each of the RuP_nDMB and RuP_nQ complexes are nearly identical. Furthermore, emission spectra for all of the complexes studied are very similar to spectra for other Ru-2,2′-bipyridine complexes, indicating that the luminescence emanates from a $d\pi$ Ru → π^* bpy MLCT excited state.[31]

Emission quantum yields for the various Ru complexes were determined in CH_2Cl_2 solution; the yields in Table I are reported relative to the model complex, RuNAc.[32] Emission yields for the RuP_nDMB complexes are in each case equal to or slightly greater than the yield for RuNAc. This demonstrates that the DMB group does not quench the MLCT excited state, consistent with the predictions from the electrochemical experiments. The enhanced emission yields noted for the RuP_nDMB series relative to RuNAc are attributed to an effect of the peptide or DMB group upon the nonradiative decay rate of the MLCT excited state.[33]

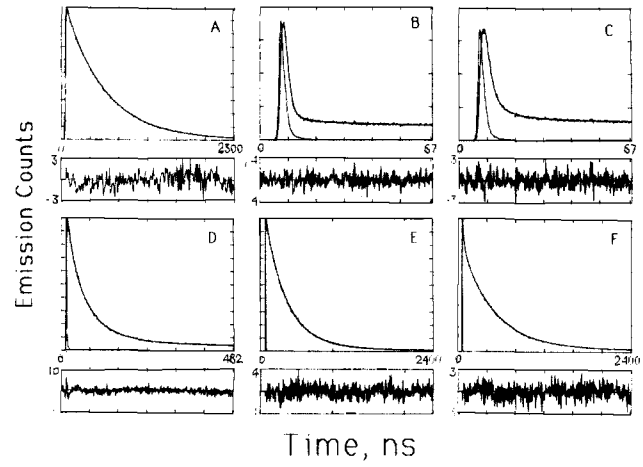

Figure 1. Time resolved emission decays in vacuum degassed CH_2Cl_2 solution, λ_{ex} = 400 nm, λ_{em} = 600 nm. Upper boxes show the experimental decays and the calculated fits. Lower boxes show plots of the weighted residuals. (A) RuNAc, time scale 0–2300 ns. (B) RuQ, time scale 0–67 ns. (C) RuP_1Q, time scale 0–67 ns. (D) RuP_2Q, time scale 0–482 ns. (E) RuP_3Q, time scale 0–2400 ns. (F) RuP_4Q, time scale 0–2400 ns.

Emission quantum yields for the RuP_nQ complexes are in each case reduced relative to RuNAc. Furthermore, the yields follow the trend, $RuQ \approx RuP_1Q < RuP_2Q < RuP_3Q < RuP_4Q <$ RuNAc. This result indicates that the quinone quenches *Ru and that the quenching efficiency decreases with an increase in the number of peptide residues that separate the Ru and quinone sites. The quenching is attributed to an intramolecular Ru to quinone electron transfer (k_{et} process, Scheme I) which competes with normal radiative and nonradiative decay of the MLCT excited state (k_d process, Scheme I). The trend in luminescence yields for the RuP_nQ system indicates qualitatively that the electron transfer rate decreases as the number of peptide spacers increases.

The rate for intramolecular electron transfer could be calculated from the emission yield data for the RuP_nQ system if Scheme I is assumed and if *Ru to quinone electron transfer is irreversible.[34] However, in the short peptide homologues (e.g., n = 0, 1, and 2), excited state quenching is almost complete, and the overall emission yield is strongly affected even by a small amount of a luminescent impurity. Thus, if luminescent impurities are present, calculation of k_{et} from emission yields will result in underestimated values. Multiexponential analysis of time-resolved emission allows separation of the short-lived RuP_nQ emission components from the long-lived impurity emission. For this reason, time-resolved data rather than the emission yield data are used to estimate electron transfer rates (vide infra).

Emission Lifetime Studies. Lifetimes for MLCT luminescence from RuNAc and the RuP_nDMB and RuP_nQ complexes in CH_2Cl_2 solution were measured with use of time-correlated single-photon counting.[35] Figure 1 shows the decay for RuNAc and the RuP_nQ series for comparison. Table II gives the results of computer fits of the experimental decay profiles.

Figure 1A shows the emission decay profile of RuNAc with the computer calculated fit superimposed; Table II contains the parameters for the fit. The RuNAc decay is described well by a single exponential function with a lifetime of 530 ns as indicated

(29) The equations used for calculation of the excited state potentials are as follows: $E_{1/2}(*Ru^{2+}/Ru^{3+}) = E_{1/2}(R^{2+}/Ru^{3+}) - E_{MLCT}$; $E_{1/2}(*Ru^{2+}/Ru^{+}) = E_{1/2}(Ru^{2+}/Ru^{+}) + E_{MLCT}$.
(30) Breslow, R. *Pure Appl. Chem.* **1974**, *40*, 493–509.
(31) Watts, R. J. *J. Chem. Educ.* **1983**, *60* 834–842.
(32) The quantum yield of emission for RuNAc is 0.042.
(33) This hypothesis is based on the observation that the radiative decay rate, calculated by ϕ_{em}/τ_{em}, is constant for the RuP_nDMB series.
(34) Under these assumptions, $k_{et} = (\phi^0_{em} - \phi_{em})/\phi_{em}\tau^0$, where ϕ^0_{em} and τ^0 are respectively the emission yield and lifetime of the unquenched Ru chromophore and ϕ_{em} is the emission yield of the RuP_nQ complex.
(35) O'Connor, D. V.; Phillips, D. *Time-correlated Single Photon Counting*; Academic: New York, 1984.

Table II. Emission Decay Lifetimes, CH_2Cl_2 Solution[a,b]

	RuNAc		RuP_nDMB		RuP_nQ						
n	τ, ns	$R\chi^2$	τ, ns	$R\chi^2$	τ_1, ns	α_1	τ_2, ns	α_2	τ_3, ns	α_3	$R\chi^2$
0	530	1.189	578	1.102	550	0.04	17.7	0.01	1.0	0.95	1.048
1			—	—	550	0.08	10.9	0.05	1.8	0.87	0.931
2			592	1.342	567	0.07	54.5	0.68	10.5	0.24	1.256
3			627	1.811	542	0.10	273	0.78	5.0	0.12	1.155
4			540	1.484	448	0.60	45.3	0.12	6.1	0.28	0.934

[a] Estimated uncertainty in lifetimes is ±5%. $R\chi^2$ is the reduced chi-square for the fit. [b] τ_i indicates lifetime of component and α_i reflects the relative amplitude of component in multiexponential fit (see ref 45).

by the low $R\chi^2$. The lifetime observed for RuNAc is similar to the lifetime of $Ru(bpy)_3^{2+}$ in CH_2Cl_2 (488 ns)[23] and is consistent with assignment of the emitting state in RuNAc to $d\pi$ Ru → π^* bpy MLCT.

The experimental emission decays for each of the RuP_nDMB complexes were fit using single-exponential functions; the calculated lifetimes and $R\chi^2$ values are summarized in the second column of Table II. The emission lifetimes of these complexes, which range from 540 to 630 ns, are all slightly larger than the emission lifetime of RuNAc. The fact that long lifetimes are observed for the RuP_nDMB complexes indicates that the DMB group does not quench the Ru MLCT excited state by electron transfer, in accord with the predictions based upon the redox potentials of *Ru and the DMB moiety. The variation in lifetimes observed for the RuP_nDMB series is likely due to an effect of the oligoproline or DMB group upon the non-radiative decay rate of the Ru MLCT excited state.[33]

Luminescence decays for the RuP_nQ complexes are markedly different from those for the "unquenched" RuNAc and RuP_nDMB complexes. Several comments can be made concerning the experimental data presented in Figure 1B–F and Table II. (1) The emission decays more rapidly for the RuP_nQ complexes than for RuNAc or the RuP_nDMB complexes. (2) The emission decay takes place on a progressively longer time scale as the length of the peptide spacer increases (compare Figure 1B–F and the lifetime components with largest amplitudes in Table II). (3) The luminescence decays do not follow first-order kinetics and require a multiexponential function for simulation.[45] The attenuation in emission lifetime observed for the RuP_nQ complexes is attributed to quenching of the Ru MLCT excited state by intramolecular electron transfer to the covalently attached quinone site. The fact that the luminescence decay becomes slower as the length of the peptide chain increases suggests that electron transfer quenching becomes less efficient as the average distance separating Ru and Q increases.

Mechanism of Electron Transfer in the RuP_nQ Complexes. Origin of Multiexponential Emission Decay. An important question that must be addressed concerns the origin of the multiexponential luminescence decays observed for the RuP_nQ complexes. However, prior to discussing the multiexponential decays in terms of properties inherent to the RuP_nQ complexes, it should be pointed out that for most of the complexes a small amplitude decay component was resolved that can be assigned to emission from an unquenched Ru chromophore. Table II shows that most of the RuP_nQ complexes (n = 0–3) display a long-lived, low-amplitude emission decay component (τ_1, Table II) that varies little with the length of the peptide spacer. The presence of this long-lived component can be visually confirmed in decay traces for RuQ and RuP_1Q (Figure 1B and C, respectively). The similarity of the τ_1 lifetime component for RuQ, RuP_1Q, RuP_2Q, and RuP_3Q with the lifetime of RuNAc strongly suggests that this component may be attributed to luminescence from an impurity that contains the unquenched Ru chromophore. (It is likely that the luminescent impurity is the corresponding RuP_nQH_2 complex that persists after oxidation, vide supra.) The situation is somewhat different for RuP_4Q, as the τ_1 component has a relatively large amplitude and a shorter lifetime than would be expected for the unquenched RuP_4QH_2 species. For RuP_4Q the τ_1 component is assigned to emission intrinsic to the quinone complex; presumably emission from RuP_4Q masks the small component expected from any residual RuP_4QH_2 which might be present, due to the similarity of the lifetimes for the two forms.

While the presence of a small component of unquenched Ru luminescence accounts in part for the multiexponential decays observed for the RuP_nQ complexes, the data in Table II show that each complex displays at least two other lifetime components in addition to the unquenched component. It is clear that the multiexponential decay behavior is due to a property intrinsic to the RuP_nQ complexes. Consideration of the mechanism of electron transfer quenching within the RuP_nQ complexes may provide insight as to the origin of the multiexponential luminescence decays. Intramolecular electron transfer within a photoexcited RuP_nQ complex would occur by either of two mechanisms. The first mechanism is electron transfer between Ru and quinone sites that are in close proximity due to folding of the peptide spacer. If quenching occurs exclusively by this mechanism, we assume that the rate determining step would be a dynamic process involving isomerization of the peptide spacer into the "correct" conformation for electron transfer. The fact that substantial quenching is observed for each of the complexes indicates that the rate-limiting step effectively competes with deactivation of the complexes via normal radiative and non-radiative decay processes that occur with $k \approx 10^6$ s^{-1}. Therefore, in order for this mechanism to be important, conformational isomerization of the peptide spacer would have to be a relatively rapid process, occurring with $k > 10^5$ s^{-1}. However, this is inconsistent with studies on the conformational isomerization of proline containing peptides which indicate that peptide conformational isomerization is relatively slow,[36] occurring several orders of magnitude more slowly than required under the kinetic constraints mentioned above.

The second mechanism for quenching is long-range electron transfer[2] from Ru to Q across the peptide bridges. If long-range electron transfer is the the preferred mechanism for intramolecular quenching, then it may be assumed that the factor that determines the electron transfer rate is the separation distance between Ru and the quinone.[2,14a] An attractive feature of the long-range transfer mechanism is that it provides an explanation for the multiexponential kinetics. Consider a situation in which (for a given peptide length) the spacers exist in several different, slowly interconverting conformational forms. This would result in an ensemble of molecules with a distribution of Ru to quinone separation distances. The luminescence decay kinetics for such a system would be multiexponential, reflecting the fact that electron transfer occurs with a range of rate constants as a result of the distribution in separation distance between the Ru and quinone sites.[37]

It is a well-established fact that in nonpolar organic solution oligoprolines exist as a mixture of conformational isomers.[38] Indeed, NMR experiments designed to study peptide conformations in the bridged Ru complexes (under conditions similar to those used in the photophysical experiments) provide clear evidence for the existence of slowly interconverting conformational isomers.[39] Because luminescence experiments on the RuP_nQ com-

(36) Cheng, H. N.; Bovey, F. A. *Biopolymers* **1977**, *16*, 1465–1472.
(37) (a) James, D. R.; Ware, W. R. *Chem. Phys. Lett.* **1985**, *120*, 455–459. (b) James, D. R.; Liu, Y.-S.; DeMayo, P.; Ware, W. R. *Chem. Phys. Lett.* **1985**, *120*, 460–465.
(38) (a) Chao, Y.-Y. H.; Bersohn, R. *Biopolymers* **1978**, *17*, 2761–2767. (b) Grathwohl, C.; Wüthrich, K. *Biopolymers* **1976**, *15*, 2025–2041. (c) Grathwohl, C.; Wüthrich, K. *Biopolymers* **1976**, *15*, 2043–2057. (d) Deber, C. M.; Bovey, F. A.; Carver, J. P.; Blout, E. R. *J. Am. Chem. Soc.* **1970**, *92*, 6191–6198.

Table III. Estimated Intramolecular Electron Transfer Rates[a]

complex	k_{et}, s^{-1}
RuQ	1.0×10^9
RuP_1Q	5.6×10^8
RuP_2Q	1.7×10^7
RuP_3Q	2.1×10^6
RuP_4Q	3.8×10^5

[a] Calculated with eq 1, see text.

plexes were conducted in a relatively nonpolar organic solvent, it is no surprise that the decay kinetics is complicated due to the existence of multiple conformational isomers.

A logical solution to the problem of multiple peptide conformational isomers in the bridged complexes would be to conduct the experiments in aqueous solution, conditions that have been demonstrated to stabilize oligoprolines in a single, extended conformation.[10c] Unfortunately, attempts to study the luminescence of the RuP_nQ complexes in protic solvents under a variety of conditions have been unsuccessful due to the fact that the quinone becomes reduced, apparently by reaction with the solvent.[40]

The experimental evidence suggests that intramolecular quenching in the RuP_nQ complexes occurs predominantly via long-range electron transfer across the peptide bridges. We conclude that (1) the complexity in the luminescence decay kinetics is due in part to the existence of multiple conformational isomers of the peptide bridges and (2) the increase in the average emission lifetime with increasing peptide length is the result of a decrease in k_{et} as the average Ru to quinone separation distance becomes larger.

Estimation of Intramolecular Electron Transfer Rates for the RuP_nQ Complexes. From the preceding discussion it is apparent that the complexity observed in the luminescence decay kinetics is a manifestation of the fact that intramolecular electron transfer occurs with a range of rate constants for a given peptide spacer length. This makes it difficult to assess the quantitative dependence of k_{et} on the peptide spacer length. Despite this shortcoming, the luminescence data for the RuP_nQ system suggest a strong dependence of the average efficiency of electron transfer upon the peptide spacer length. Therefore, it is worthwhile to use the emission decay data to provide a qualitative indication of the variation in k_{et} with the peptide spacer length.

As a working hypothesis, we suggest that the luminescence lifetime component with the largest amplitude represents the lifetime of the conformational form of the RuP_nQ complex which predominates in solution. Within this model, the average rate constant for electron transfer can be calculated as[13-17]

$$k_{et} = \frac{1}{\tau} - \frac{1}{\tau^0} \qquad (1)$$

where τ is the lifetime component with the largest amplitude for the RuP_nQ complex and τ^0 is the lifetime of the unquenched Ru chromophore. Average intramolecular electron transfer rate constants for the RuP_nQ complexes have been calculated with use of the lifetimes of the corresponding RuP_nDMB species for τ^0; the data are compiled in Table III. The trend that is observed in k_{et} indicates that, on the average, the rate decreases by a factor of almost 10 for each added amino acid spacer. This relatively strong dependence of the rate upon the peptide bridge length is qualitatively consistent with recent experiments on long-range electron transfer that suggest an exponential dependence of the rate on distance.[2a] Unfortunately, with the present system it is not possible to make a quantitative statement regarding the distance dependence of electron transfer owing to the uncertainty in the Ru to quinone separation distance in the peptide bridged molecules.[41]

Conclusion

The chromophore-quencher molecules, RuP_nQ, were prepared and characterized for the purpose of examining the distance dependence of photoinduced electron transfer in a peptide-bridged system. Luminescence experiments demonstrate that the yield and lifetime of emission from the Ru complex are quenched substantially in the RuP_nQ complexes relative to the RuNAc and RuP_nDMB model complexes. The quenching is attributed to electron transfer from the Ru MLCT excited state to the quinone, based upon the fact that the process is exothermic by $\approx$0.35 eV. Although the luminescence experiments qualitatively indicate that the efficiency for electron transfer quenching falls as the number of peptide spacers increases, quantitative determination of the dependence of electron transfer rate upon distance is not possible owing to the fact that emission decays for the RuP_nQ complexes display multiexponential kinetics. The multiexponential decays are attributed to the existence of a number of different, slowly equilibrating conformational isomers for the peptide bridges in the relatively nonpolar CH_2Cl_2 solvent environment, a situation that leads to a distribution of Ru to quinone separation distances for a given peptide spacer length. Work in progress seeks to examine photoinduced intramolecular electron transfer in a peptide-bridged system that can be studied in water, a solvent environment in which the peptide spacers preferentially adopt a single extended conformation.[10c]

Experimental Section

General Synthetic. Solvents and chemicals used for synthesis were of reagent grade and used without purification unless noted. CH_2Cl_2, CH_3CN, and CH_3COCH_3 were distilled from P_2O_5, CaH_2, and $MgSO_4$ respectively and stored over molecular sieves. Triethylamine was distilled from KOH and DDQ was vacuum sublimed before use. Merck silica gel (230–400 mesh) was used for flash chromatography. Neutral alumina (150 mesh, Brockman I, Aldrich Chemical) was deactivated by adding 6% H_2O before use in chromatography of the metal complexes. ^1H and ^{13}C NMR spectra were recorded on a 200-MHz instrument equipped with a Bruker magnet and a Nicolet 1180 data system with electronics assembled in house. Elemental analyses were conducted by the U.C. Berkeley Chemistry Analytical Facility. UV–visible spectra were recorded on Varian 2300 and HP 8450A spectrophotometers. IR spectra were recorded on a Perkin-Elmer 283 spectrophotometer. FTIR spectra were recorded on a Nicolet 5DX spectrometer.

DMB(L-Pro)$_1$OH. To a solution of 1.2 g of HCl·H(L-Pro)OBz (5 mmol, Sigma Chemical Co.) in 40 mL of CH_2Cl_2 was added 1.2 g of triethylamine (12 mmol). Then 1.6 g of 2,5-dimethoxyphenylacetyl chloride (7.5 mmol) was added. This solution was stirred overnight under a drying tube. On the following day the solution was filtered and the CH_2Cl_2 removed by rotary evaporation. DMB(L-Pro)OBz was isolated by extracting a $CHCl_3$ solution with 1 N HCl and 5% $NaHCO_3$. Purification was effected by flash chromatography (4% MeOH/$CHCl_3$). Then the OBz protecting group was removed by catalytic hydrogenation.[42] The product was obtained as a colorless oily liquid; yield 0.35 g (24%). Spectral data: IR ($CHCl_3$) 3200–2700, 3030, 2970, 2890, 2830, 1750, 1640, 1600, 1510, 1450, 1310, 1290, 1225, 1050, 670 cm^{-1}; ^1H NMR ($CDCl_3$) δ 1.9–2.2 (m, 4 H, β–γ proline CH_2CH_2), 3.4–3.7 (m, 2 H, δ proline CH_2), 3.69 (d, 2 H, benzylic CH_2), 3.76 (s, 3 H, OCH_3), 3.78 (s, 3 H, OCH_3), 4.70 (m, 1 H, α proline CH), 6.8 (s, 3 H, DMB aromatic).

DMB(L-Pro)$_2$OH. The derivatized dipeptide was prepared from HCl·H(L-Pro)$_2$OBz[38d,42] by the method described for DMB(L-Pro)$_1$OH. DMB(L-Pro)$_2$OH was obtained as a white amorphous solid; yield 0.8 g (40%). Spectral data: IR ($CHCl_3$) 3200–2700, 3010, 2890, 2845, 1760, 1640, 1510, 1450, 1330, 1230, 1050, 660 cm^{-1}; ^1H NMR ($CDCl_3$) δ 1.8–2.4 (m, 8 H, 2 × β–γ proline CH_2CH_2), 3.5–4.0 (m, 4 H, 2 × δ proline CH_2), 3.50 (s, 2 H, benzylic CH_2), 3.76 (s, 3 H, OCH_3), 3.78 (s,

(39) The β and γ proline carbons appear as doublets in ^{13}C NMR spectra of the RuP_nQH_2 complexes in CD_3CN solution. This splitting has been attributed to the existence of slowly interconverting (cis and trans) peptide conformational isomers (ref 38).

(40) ^1H NMR shows that when RuQ is dissolved in D_2O the quinone ring proton resonances dissappear and a new set of resonances appear in the aromatic region. The chemical shifts and splitting pattern of the new aromatic resonances are consistent with the formation of a hydroquinone species.

(41) Experimental and theoretical evidence suggests that $k_{et} = \nu_0 \exp[-\beta r]$, where ν_0 is the rate when donor and acceptor are in contact, r is the internuclear separation distance, and β expresses the dependence of k_{et} on r (ref 2). If we assume that the incremental increase in distance between Ru and Q is 3.1 Å per proline residue (ref 10c), then $\beta \approx 0.75$ Å^{-1} can be deduced from the data in Table III. It should be stressed, however, that this β value at best represents only a lower limit for the true value in the RuP_nQ system.

(42) Miyoshi, M.; Kimura, T.; Sakakibara, S. *Bull. Chem. Soc. Jpn.* **1970**, *43*, 2941–2944.

3 H, OCH_3). 4.6–4.7 (m, 2 H. 2 × α proline CH), 6.7–6.9 (m, 3 H. DMB aromatic).

DMB(L-Pro)$_3$OH. The derivatized tripeptide was prepared from HCl·H(L-Pro)$_3$OBz[38d,42] by the method described for DMB(L-Pro)$_1$OH. DMB(L-Pro)$_3$OH was obtained as a white amorphous solid; yield 0.97 g (40%). Spectral data: IR ($CHCl_3$) 3200–2700, 3020, 2890, 2850, 1760, 1735, 1650, 1510, 1440, 1330, 1220, 1050, 660 cm^{-1}; ^1H NMR ($CDCl_3$) δ 1.7–2.3 (m, 12 H, 3 × β–γ proline CH_2CH_2), 3.4–4.0 (m, 6 H, 3 × δ proline CH_2), 3.70–3.75 (m, 8 H, 2 × OCH_3, benzylic CH_2), 4.50–4.75 (m, 3 H, 3 × α proline CH), 6.7–6.9 (m, 3 H, DMB aromatic).

DMB(L-Pro)$_4$OH. The derivatized tetrapeptide was prepared from HCl·H(L-Pro)$_4$OBz[38d,42] by the method described for DMB(L-Pro)$_1$OH. DMB(L-Pro)$_4$OH was obtained as an amorphous white solid; yield 1.9 g (65%). Spectral data: IR ($CHCl_3$) 3200–2700, 3010, 2890, 2850, 1750, 1645, 1510, 1445, 1330, 1210, 1050, 660; ^1H NMR ($CHCl_3$) δ 1.8–2.3 (m, 16 H, 4 × β–γ proline CH_2CH_2), 3.4–4.0 (m, 8 H, 4 × δ proline CH_2), 3.7–3.8 (m, 8 H, 2 × OCH_3, benzylic CH_2), 4.5–4.8 (m, 4 H, 4 × α proline CH), 6.7–6.9 (m, 3 H, DMB aromatic).

RuNAc. To a solution of 300 mg of $[(bpy)_2Ru(5\text{-}AP)][PF_6]_2$[43] (0.33 mmol) and 73 mg of triethylamine (0.72 mmol) in 10 mL of CH_2Cl_2 was added 265 mg of CH_3COCl (3.4 mmol). The solution was stirred overnight at 25 °C. On the following day the solvent was removed by rotary evaporation and the product was dissolved in H_2O and precipitated by addition of NH_4PF_6. The material was collected, dried under vacuum, and then chromatographed on alumina with 30% CH_3CN/CH_2Cl_2 solvent. After chromatography the complex was dissolved in CH_3CN and reprecipitated from diethyl ether. The product was obtained as a bright orange powder; yield 200 mg (64%). Spectral data: FTIR (KBr) 3600–3200 br, 3110, 1696, 1532, 1468, 1448, 1428, 845, 765, 735, 560 cm^{-1}; ^1H NMR (CD_3CN) δ 2.3 (s, 3 H, CH_3), 7.17–7.28 (m, 2 H, aromatic), 7.37–7.50 (m, 2 H, aromatic), 7.50–7.60 (m, 2 H, aromatic), 7.64–7.87 (m, 4 H, aromatic), 7.94–8.15 (m, 6 H, aromatic), 8.45–8.63 (m, 6 H, aromatic), 8.73 (dd, 1 H, aromatic) 8.90 (s, 1 H, NH); UV-vis (CH_3CN) λ 450 (ε14 400), 284 (59 500), 276 (sh, 57 600), 245 (36 200).

Anal. Calcd for $C_{34}H_{27}N_7O_1Ru_1P_2F_{12}\cdot H_2O$: C, 42.59; H, 3.05; N, 10.23. Found: C, 42.44; H, 2.80; N, 10.07.

RuDMB. To a solution of 300 mg of $[(bpy)_2Ru(5\text{-}AP)][PF_6]_2$ (0.33 mmol) and 80 mg of triethylamine (0.80 mmol) in 10 mL of CH_2Cl_2 was added 86 mg of 2,5-dimethoxyphenylacetyl chloride (0.4 mmol). The solution was stirred for 2 days at 25 °C and then refluxed for 2 h. After cooling, the solvent was removed by rotary evaporation and the product was dissolved in H_2O and then precipitated by adding NH_4PF_6. The crude product was dried under vacuum and purified by alumina chromatography with 30% CH_3CN/CH_2Cl_2 solvent. After chromatography the complex was dissolved in CH_3CN and precipitated from diethyl ether. The product was obtained as a bright orange powder; yield 210 mg (59%). Spectral data: ^1H NMR (CD_3CN) δ 3.75 (s, 3 H, OCH_3), 3.86 (s, 2 H, benzylic CH_2), 3.87 (s, 3 H, OCH_3), 6.80–6.90 (dd, 1 H, DMB aromatic), 6.90–7.05 (m, 2 H, DMB aromatic), 7.20–7.30 (m, 2 H, aromatic), 7.40–7.50 (m, 2 H, aromatic), 7.50–7.67 (m, 2 H, aromatic), 7.60–7.90 (m, 4 H, aromatic), 7.90–8.20 (m, 6 H, aromatic), 8.40–8.70 (m, 7 H, aromatic), 8.95 (s, 1 H, NH); UV-vis (CH_3CN) λ 450 (ε 15 600), 284 (66 200), 276 (sh, 63 600), 244 (39 000).

RuP$_1$DMB. $[(bpy)_2Ru(5\text{-}AP)][PF_6]_2$ (400 mg, 0.44 mmol), DMB-(L-Pro)$_1$OH (260 mg, 0.88 mmol), and dicyclohexylcarbodiimide (360 mg, 1.76 mmol) were dissolved in a mixture of 9 mL of CH_2Cl_2 and 1 mL of CH_3CN. The solution was stirred for 2 days at 25 °C. Then the solution was filtered and the solvent evaporated. The product was dissolved in a minimal amount of CH_3CN and centrifuged to remove insoluble byproducts. The supernatant was placed onto an alumina column and chromatographed with 30% CH_3CN/CH_2Cl_2 solvent. After chromatography the product was dissolved in CH_3CN and precipitated from diethyl ether. The product was obtained as a bright orange powder; yield 220 mg (42%). Spectral data: ^1H NMR (CD_3CN) δ 1.90–2.25 (m, 4 H, β–γ proline CH_2CH_2), 3.35–3.80 (m, 10 H, benzylic CH_2, 2 × OCH_3, δ proline CH_2), 4.80–4.90 (m, 1 H, α proline CH), 6.50–6.80 (m, 3 H, DMB aromatic), 7.18–7.27 (m, 2 H, aromatic), 7.37–7.48 (m, 2 H, aromatic), 7.49–7.55 (m, 2 H, aromatic), 7.60–7.88 (m, 4 H, aromatic), 7.92–8.13 (m, 6 H, aromatic), 8.42–8.60 (m, 6 H, aromatic), 8.70 (d, 1 H, aromatic), 10.40 (d, 1 H NH).

RuP$_2$DMB. This complex was prepared from $[(bpy)_2Ru(5\text{-}AP)][PF_6]_2$ and DMB(L-Pro)$_2$OH by the method described for RuP$_1$DMB. The product was obtained as a bright orange powder; yield 171 mg (30%). Spectral data: ^1H NMR (CD_3CN) δ 1.75–2.40 (m, 8 H, 2 × β–γ proline CH_2CH_2), 3.20–3.75 (m, 12 H, benzylic CH_2, 2 × OCH_3, 2 × δ proline CH_2), 4.57–4.88 (m, 2 H, 2 × α proline CH), 6.52–6.90 (m, 3 H, DMB aromatic), 7.15–7.35 (m, 2 H, aromatic), 7.40–7.50 (m, 2 H, aromatic), 7.51–7.62 (m, 2 H, aromatic), 7.63–7.77 (m, 2 H, aromatic), 7.79–7.90 (m, 2 H, aromatic), 7.92–8.18 (m, 6 H, aromatic), 8.45–8.65 (m, 6 H, aromatic), 8.78 (dd, 1 H aromatic), 10.02 (s, 1 H, NH); UV-vis (CH_3CN) λ 450 (ε 14 900), 284 (63 300), 276 (sh, 59 900), 244 (38 800).

RuP$_3$DMB. This complex was prepared from $[(bpy)_2Ru(5\text{-}AP)][PF_6]_2$ and DMB(L-Pro)$_3$OH by the method described for RuP$_1$DMB. The product was obtained as a bright orange powder; yield 200 mg (33%). Spectral data: ^1H NMR (CD_3CN) δ 1.70–2.50 (m, 12 H, 3 × β–γ proline CH_2CH_2), 3.00–3.90 (m, 14 H, benzylic CH_2, 2 × OCH_3, 3 × δ proline CH_2), 4.50–4.85 (m, 3 H, 3 × α proline CH), 6.20–6.90 (m, 3 H, DMB aromatic), 7.15–7.30 (m, 2 H, aromatic), 7.35–7.50 (m, 2 H, aromatic) 7.50–7.60 (m, 2 H, aromatic), 7.65–7.85 (m, 4 H, aromatic), 7.90–8.20 (m, 6 H, aromatic), 8.30–8.60 (m, 6 H, aromatic), 8.70 (dd, 1 H, aromatic), 10.00 (d, 1 H, NH); UV-vis (CH_3CN) λ 450 (ε 14 700), 284 (62 100), 276 (sh, 58 600), 244 (35 000).

RuP$_4$DMB. This complex was prepared from $[(bpy)_2Ru(5\text{-}AP)][PF_6]_2$ and DMB(L-Pro)$_4$OH by the method described for RuP$_1$DMB. The product was obtained as a bright orange powder; yield 260 mg (40%). Spectral data: ^1H NMR (CD_3CN), δ 1.60–2.50 (m, 16 H, 4 × β–γ proline CH_2CH_2), 3.35–3.80 (m, 16 H benzylic CH_2, 2 × OCH_3, 4 × δ proline CH_2), 4.40–4.90 (m, 4 H, 4 × α proline), 6.50–6.90 (m, 3 H, DMB aromatic), 7.15–7.30 (m, 2 H, aromatic), 7.38–7.51 (m, 2 H, aromatic), 7.51–7.60 (m, 2 H, aromatic), 7.63–7.90 (m, 4 H, aromatic), 7.92–8.20 (m, 6 H, aromatic), 8.40–8.80 (m, 7 H, aromatic), 10.00 (d, 1 H, NH); UV-vis (CH_3CN) λ 450 (ε 14 400), 284 (61 000), 276 sh, 58 200), 244 (34 00).

RuQH$_2$. The reaction followed literature procedures for demethylation of methoxybenzenes. RuDMB (200 mg, 0.18 mmol) was placed in a well-dried 100-mL three-necked flask fitted with a thermometer and a 500 mL addition funnel. The flask was outgassed with dry N_2 and 10 mL of CH_2Cl_2 was added. This solution was cooled to −70 °C with a dry ice/acetone bath and then 9.0 mL of a 1.0 M BBr_3 solution in CH_2Cl_2 (9.0 mmol) was slowly added via the addition funnel. The resulting solution was stirred at −70 °C for 4 h. (During this time much of the Ru complex precipitated out of solution.) After this period the solution was warmed to 0 °C for 30 min and then 20 mL of MeOH was slowly added via the dropping funnel. The solvent was removed by rotary evaporation and an additional 50 mL of MeOH was added and then the solvent was again evaporated. The resulting red solid was dissolved in H_2O and precipitated by addition of NH_4PF_6. The complex was collected and dried under vacuum. The product was purified by alumina chromatography with use of gradient elution (50% CH_2Cl_2/CH_3CN, 100% CH_3CN, 10% MeOH/CH_3CN). Ru-containing impurities (red-orange color) were washed off prior to addition of MeOH to the mobile phase; the linked QH_2 product required MeOH in the mobile phase for elution from the column. After collection the product was redissolved in CH_3CN and precipitated from diethyl ether. $RuQH_2$ was obtained as a bright orange solid; yield 70 mg (37%). (Samples for spectroscopic experiments were chromatographed twice.) Spectral data: FTIR (KBr) 3600–2700, 1692, 1660, 1531, 1517, 1467, 1448, 1427, 840, 765, 725, 560 cm^{-1}; ^1H NMR (CD_3CN) δ 3.44 (s, 2 H, OH), 3.84 (s, 2 H, benzylic CH_2), 6.62 (dd, 1 H, QH_2 aromatic), 6.78 (m, 2 H, QH_2 aromatic), 7.17–7.28 (m, 2 H, aromatic), 7.39–7.49 (m, 2 H, aromatic), 7.50–7.58 (m, 2 H, aromatic), 7.62–7.88 (m, 4 H, aromatic), 7.93–8.17 (m, 6 H, aromatic), 8.43–8.61 (m, 6 H, aromatic), 8.67 (d, 1 H, aromatic), 9.24 (s, 1 H, NH); UV-vis (CH_3CN) λ 450 (ε 16 400), 284 (68 100), 276 (sh, 64 300), 244 (42 800).

Anal. Calcd for $C_{40}H_{31}N_7O_3Ru_1P_2F_{12}\cdot H_2O$: C, 45.03; H, 3.12; N, 9.19. Found: C, 44.84; H, 2.74; N, 8.84.

RuP$_1$QH$_2$. This complex was prepared from RuP$_1$DMB as described for $RuQH_2$. RuP$_1$QH$_2$ was a bright orange powder; yield 90 mg (46% based upon 200 mg of RuP$_1$DMB starting material). Spectral data: FTIR (KBr) 3600–2600, 2970, 2890, 1695, 1658, 1632, 1465, 1448, 1428, 845, 765, 730, 560 cm^{-1}; ^1H NMR (CD_3CN) δ 1.9–2.4 (m, 4 H, β–γ proline CH_2CH_2), 3.50–3.95 (m, 6 H, benzylic CH_2, 2 × OH, δ proline CH_2), 4.76–4.85 (m, 1 H, α proline CH), 6.45–6.80 (m, 3 H, QH_2 aromatic), 7.17–7.30 (m, 2 H, aromatic), 7.39–7.50 (m, 2 H, aromatic), 7.50–7.60 (m, 2 H, aromatic), 7.61–7.76 (m, 2 H, aromatic), 7.79–7.90 (m, 2 H, aromatic), 7.93–8.22 (m, 6 H, aromatic), 8.43–8.70 (m, 7 H, aromatic), 10.00 (s, 1 H, NH); UV-vis (CH_3CN) λ 450 (ε 17 000), 284 (73 400), 276 (sh, 69 200), 244 (45 000).

Anal. Calcd for $C_{45}H_{38}N_8O_4Ru_1P_2F_{12}\cdot 2H_2O$: C 45.72; H, 3.59; N, 9.48. Found: C, 45.72; H, 3.12; N, 9.51.

RuP$_2$QH$_2$. This complex was prepared from RuP$_2$DMB as described for $RuQH_2$. RuP$_2$QH$_2$ was a bright orange powder; yield 80 mg (41% based upon 200 mg of RuP$_2$DMB starting material). Spectral data: FTIR (KBr) 3600–2700, 2980, 2890 1692, 1632, 1605, 1465, 1448, 1429, 845, 765, 730, 560 cm^{-1}; ^1H NMR (CD_3CN) δ 1.70–2.40 (m, 8 H, 2 × β–γ proline CH_2CH_2), 3.30–3.85 (m, 8 H, benzylic CH_2, 2 × OCH_3, 2

(43) Ellis, C. D.; Margerum, L. D.; Murray, R. W.; Meyer, T. J. *Inorg. Chem.* **1983**, *22*, 1283–1291.

× δ proline CH_2), 4.52–5.00 (m, 2 H, 2 × α proline CH), 6.30–6.70 (m, 3 H, QH_2 aromatic), 7.15–7.30 (m, 2 H, aromatic), 7.36–7.50 (m, 2 H, aromatic), 7.50–7.60 (m, 2 H, aromatic), 7.60–7.78 (m, 2 H, aromatic), 7.79–7.90 (m, 2 H aromatic), 7.92–8.17 (m, 6 H, aromatic), 8.40–8.60 (m, 6 H, aromatic), 8.71 (d, 1 H, aromatic), 10.05 (s, 1 H, NH). UV-vis (CH_3CN) λ 450 (ε 15 800), 284 (65 500), 276 (sh, 63 300), 244 (42 400).

Anal. Calcd for $C_{50}H_{45}N_9O_5Ru_1P_2F_{13}\cdot 2H_2O$: C, 46.94; H, 3.87; N, 9.86. Found: C, 47.10; H, 3.49; N, 9.87.

RuP_3QH_2. This complex was prepared from RuP_3DMB by the method described for $RuQH_2$. RuP_3QH_2 was a bright orange powder; yield 137 mg (35% based upon 400 mg of RuP_3DMB starting material). Spectral data: FTIR (KBr) 3600–2700, 2985, 2890, 1692, 1635, 1605, 1464, 1448, 1429, 845, 765, 730, 560 cm^{-1}; ^1H NMR (CD_3CN) δ 1.70–2.60 (m, 12 H, 3 × β–γ proline CH_2CH_2), 3.20–3.90 (m, 8 H, benzylic CH_2 3 × δ proline CH_2), 4.40–5.05 (m, 3 H, 3 × α proline CH), 6.20–6.70 (m, 2 H, aromatic), 7.50–7.58 (m, 2 H, aromatic), 7.59–7.77 (m, 2 H, aromatic), 7.78–7.88 (m, 2 H, aromatic), 7.92–8.17 (m, 6 H, aromatic), 8.40–8.68 (m, 6 H, aromatic), 8.73 (d, 1 H, aromatic), 9.90–10.00 (m, 1 H, NH); UV-vis (CH_3CN) λ 450 (ε 15 900), 284 (65 400), 276 (sh, 62 800), 244 (40 900).

Anal. Calcd for $C_{55}H_{52}N_{10}O_6Ru_1P_2F_{12}\cdot 2H_2O$: C, 48.00; H, 4.11; N, 10.18. Found: C, 47.97; H, 3.75; N, 10.15.

RuP_4QH_2. This complex was prepared from RuP_4DMB by the method described for $RuQH_2$. RuP_4QH_2 was a bright orange powder; yield 157 mg (40% based upon 400 mg of RuP_4DMB starting material). Spectral data: FTIR (KBr) 3600–2700, 2970, 2880, 1692, 1633, 1463, 1448, 1432, 845, 765, 730, 560 cm^{-1}; ^1H NMR (CD_3CN) δ 1.60–2.50 (m, 16 H, 4 × β–γ proline CH_2CH_2), 3.20–3.90 (m, 10 H benzylic CH_2, 4 × δ proline CH_2), 4.10–5.00 (m, 4 H, 4 × α proline CH), 6.30–7.00 (m, 3 H, DMB aromatic), 7.12–7.30 (m, 2 H, aromatic), 7.35–7.90 (m, 8 H, aromatic), 7.91–8.20 (m, 6 H, aromatic), 8.35–8.80 (m, 7 H, aromatic), 9.90 (d, 1 H, NH); UV-vis (CH_3CN) λ 450 (ε 15 900), 284 (65 500), 276 (sh, 62 400), 244 (40 300).

Anal. Calcd for $C_{60}H_{59}N_{11}O_7Ru_1P_2F_{12}\cdot 3H_2O$: C, 48.32; H, 4.40; N, 10.33. Found: C, 48.47; H, 3.98; N, 10.31.

RuP_nQ. The quinone complexes were obtained by oxidation of the corresponding hydroquinone species with 2,3-dichloro-5,6-dicyanoquinone (DDQ). A mixture of the RuP_nQH_2 complex and a 5-fold molar excess of DDQ were dissolved in a minimum volume of dry acetone. The solution was allowed to stand in the dark for several hours. Separation of the oxidized metal complex, RuP_nQ, from the organic byproducts was effected by dropping the acetone reaction solution into an excess of stirred diethyl ether. This procedure resulted in precipitation of the metal complex while the organic byproducts remained in solution. The purified RuP_nQ complex was collected on a glass frit and dried in vacuo. The above procedures were carried out under dry argon. UV analysis clearly showed that the oxidzed complexes were free of organic impurities. DDQ oxidation produced materials that were 90–95% RuP_nQ as determined by NMR and UV-vis analysis; the remaining Ru was present as the corresponding RuP_nQH_2 species. Attempts to purify the RuP_nQ complexes by chromatography resulted in further contamination of the samples with strongly luminescent impurities due to reduction of the quinone. As a result, the RuP_nQ complexes were used in spectroscopic experiments immediately after ether precipitation.

Each of the RuP_nQ complexes was characterized by ^1H NMR (CD_3CN solution) and UV-vis spectroscopy (CH_2Cl_2 solution). NMR spectra of the RuP_nQ complexes were identical with spectra for the corresponding RuP_nQH_2 species except for changes in signals associated with the quinone protons. In each case quinone protons appeared as a multiplet at δ 6.70–6.80 with an integral corresponding to 3 protons. The UV-vis spectra of the RuP_nQ complexes were carefully compared to spectra of the corresponding RuP_nQH_2 species. In each case there was no change in extinction coefficient, bandshape, or position of the visible MLCT absorption (450 nm) concurrent with oxidation. However, significant changes were noticed in the UV region which were dominated by an increase in absorptivity at 245 nm following DDQ oxidation. The changes in the UV region induced by oxidation were examined by plotting difference absorption spectra (RuP_nQ minus RuP_nQH_2); in each case the difference spectra were identical with published difference spectra for similar quinone/hydroquinone systems.[27,28]

Electrochemistry. Cyclic voltammetry was conducted on a PAR 173 polarographic analyzer and a PAR 175 function generator. All electrochemistry was carried out in a single-compartment cell that was outgassed with dry N_2. Pt disk working, Pt wire auxilliary, and SSCE reference electrodes were utilized. Solutions were in CH_3CN with 0.1 M tetraethylammonium perchlorate as supporting electrolyte.

Luminescence Measurements. Solvents used in emission experiments were Burdick and Jackson spectroquality. Sample concentrations were ≈1 × 10^{-5} M, with optical densities at 450 nm ≈ 0.2. The solutions were degassed by at least 3 freeze–pump–thaw cycles and sealed at 10^{-5} Torr. The UV–visible absorption spectra of the solutions used in luminescence experiments were measured before and after collection of steady state and time resolved data. In every case the spectra were identical before and after the experiments, indicating that sample degradation did not occur during data acquisition.

Corrected emission spectra were measured on a modified Spex Fluorolog; emission intensities were determined on an in-house built steady state photon counting system. Emission intensities for vacuum degassed solutions of all of the new compounds (RuNAc, RuP_nDMB, and RuP_nQ) were measured with respect to $Ru(bpy)_3^{2+}$ in H_2O (concentration = 1 × 10^{-5} M, ϕ_{em} = 0.042);[23] correction was made for the difference in absorption of the sample and actinometer solutions at the excitation wavelength.

Emission decay measurements were conducted by time-correlated single-photon counting.[35] The photon timing system was similar to the nanosecond FLI system available from Photochemical Research Associates. Analysis and graphics were carried out on a VAX 11/780 computer with software developed in-house. The excitation light was filtered with Corning glass filters 4-96 and 7-59; this filter combination has a maximum transmittance at 405 nm with ≈70 nm fwhm. The fluorescence was filtered with a broad-bandpass interference filter with maximum transmittance at 600 nm. The start rate was 30 kHz and the stop rate was typically 500 Hz; however, for weakly emiting samples the stop rate was lower. Generally 10^4 counts were obtained in the maximum channel, but for weakly emitting samples (RuQ and RuP_1Q) slow stop rates precluded collecting as many counts. For these samples 3000–4000 counts were collected in the maximum channel.

Data analysis included deconvolution of the instrument response function (fwhm ≈ 2.6 ns) and the use of multiple exponentials[45] when necessary to obtain satisfactory fits of the decays. The goodness of the fits was judged by the $R\chi^2$ (reduced chi-square)[35] and by visual inspection of the plotted residuals.

Emission lifetimes of samples with decay components ≤1.0 ns were verified with use of a single-photon timing apparatus equipped with a mode-locked Ar ion laser excitation source and a microchannel plate detector. The experimental setup and operating parameters for this system have been previously described.[44] During experiments with the Ru complexes, the 460-nm line from the Ar ion laser was used for excitation. In this mode, the instrument response function had fwhm = 220 ps. Lifetimes ranging from 50 ps to 3 ns could be measured with this system.

Acknowledgment. This work was supported by the Director, Office of Energy Research, Office of Basic Energy Sciences, Division of Energy Biosciences, U.S. Department of Energy under contract DE-AC0376SF00098. K.S.S. gratefully acknowledges the Miller Institute for Basic Research, UC Berkeley for postdoctoral support. We thank Dr. Ed Orton for helpful comments and Dr. Alfred Holzwarth for assistance with the mode-locked laser experiments.

Registry No. DMB(L-Pro)$_1$OH, 112220-18-5; DMB(L-Pro)$_2$OH, 112220-19-6; DMB(L-Pro)$_3$OH, 112220-20-9; DMB(L-Pro)$_4$OH, 112220-21-0; RuNAc, 112219-92-8; RuDMB, 112219-94-0; RuP_1DMB, 112219-96-2; RuP_2DMB, 112219-98-4; RuP_3DMB, 112220-00-5; RuP_4DMB, 112220-02-7; $RuQH_2$, 112220-04-9; RuP_1QH_2, 112220-06-1; RuP_2QH_2, 112220-08-3; RuP_3QH_2, 112220-10-7; RuP_4QH_2, 112220-11-8; RuQ, 112220-13-0; RuP_1Q, 112220-15-2; RuP_2Q, 112247-00-4; RuP_3Q, 112247-02-6; RuP_4Q, 112220-17-4; DMB(L-Pro)OBz, 112220-22-1; HCl·H(L-Pro)OBz, 16652-71-4; HCl·H(L-Pro)$_2$OBz, 51211-55-3; HCl·H(L-Pro)$_3$OBz, 67550-20-3; HCl·H(L-Pro)$_4$OBz, 90704-85-1; $[(bpy)_2Ru(5\text{-}AP)]^{2+}[PF_6^-]_2$, 84537-86-0; 2,5-dimethoxyphenylacetyl chloride, 17918-14-8.

(44) (a) Haehnel, W.; Nairn, J. A.; Reisberg, P.; Sauer, K. *Biochim. Biophys. Acta* **1982**, *680*, 161–173. (b) Turko, B. T.; Nairn, J. A.; Sauer, K. *Rev. Sci. Instrum.* **1983**, *54*, 118–120.

(45) Complex luminescence decays were fitted to a multiexponential function of the form, $I(t) = \sum \alpha_i \exp[-t/\tau_i]$.